Photodissociation of Ethylene Sulfide at 193 nm: A Photofragment Translational Spectroscopy Study with VUV Synchrotron Radiation and ab Initio Calculations

Fei Qi,*,† Osman Sorkhabi,† Arthur G. Suits,‡ Siu-Hung Chien,§ and Wai-Kee Li§

Contribution from the Chemical Sciences Division, Ernest Orlando Lawrence Berkeley National Laboratory, Berkeley, California 94720, Department of Chemistry, State University of New York at Stony Brook, Stony Brook, New York 11794, and Chemistry Department, Brookhaven National Laboratory, Upton, New York 11973, and Department of Chemistry, The Chinese University of Hong Kong, Shatin, N.T., Hong Kong

Received September 8, 2000

Abstract: Photodissociation of ethylene sulfide at 193 nm has been studied using photofragment translational spectroscopy and ab initio theoretical calculations. Tunable synchrotron radiation was used as a universal but selective probe of the reaction products to reveal new aspects of the photodissociation dynamics. The channel giving S + C_2H_4 was found to be dominated by production of ground-state sulfur atoms ($S(^3P):S(^1D)$ = 1.44:1), mostly through a spin-forbidden process. The results also suggest the presence of a channel giving $S(^3P)$ in conjunction with triplet ethylene C_2H_4 ($^3B_{1u}$) and allow insight into the energy of the latter species near its equilibrium geometry, in which the two methylene groups occupy perpendicular planes. In addition, a channel leading to the production of H_2S with C_2H_2 also has been observed. Our experimental results are supported and elaborated by theoretical calculations.

1. Introduction

Ethylene sulfide, *c*-C_2H_4S, is a three-membered heterocyclic molecule with a sulfur atom. Photodissociation of ethylene sulfide can give rise to a number of interesting and important radicals, and thus its photochemistry represents a powerful means of obtaining insight into these species. Photodissociation studies of ethylene sulfide at 193 nm have shown the importance of a process yielding excited-state sulfur atoms (^1D) and ground-state ethylene (^1A_g) (process **I′**) using photofragment translational spectroscopy (PTS)[1] and Doppler-broadened laser-induced fluorescence spectroscopy.[2] The PTS study suggested that the sulfur atoms were produced mostly in their excited state $^1D_2$ with a small yield of ground-state sulfur (^3P).[1] Chin and coworkers detected S, C_2H_4, CS_2, and H_2S as the major products in the thermal decomposition study of *c*-C_2H_4S, with acetylene and thiophene observed as minor products.[3]

The absorption spectrum of ethylene sulfide shows a series of sharp resonances beginning near 192.2 nm, that have been assigned as a vibrational progression in the 4p Rydberg transition.[4] Carnell and Peyerimhoff[5] assigned this to a $4p_{(2)} \leftarrow n(b_1)$ transition making the excitation ($^1A_1 \leftarrow {}^1A_1$) in the C_{2v} representation of the molecule. The following channels are energetically accessible via photodissociation at 193 nm:

$$c\text{-}C_2H_4S + h\nu_{193\ nm} \rightarrow C_2H_4\ (^1A_g) + S\ (^1D) \qquad \Delta H_{avai} = 65\ \text{kcal/mol} \quad (I')$$

$$c\text{-}C_2H_4S + h\nu_{193\ nm} \rightarrow C_2H_4\ (^3B_{1u}) + S\ (^3P) \qquad \Delta H_{avai} = 28\ \text{kcal/mol} \quad (I'')$$

$$c\text{-}C_2H_4S + h\nu_{193\ nm} \rightarrow C_2H_4\ (^1A_g) + S\ (^3P) \qquad \Delta H_{avai} = 92\ \text{kcal/mol} \quad (I''')$$

$$c\text{-}C_2H_4S + h\nu_{193\ nm} \rightarrow H_2CCH + HS \qquad \Delta H_{avai} = 66\ \text{kcal/mol} \quad (II)$$

$$c\text{-}C_2H_4S + h\nu_{193\ nm} \rightarrow H_2CC: + H_2S \qquad \Delta H_{avai} = 75\ \text{kcal/mol} \quad (III')$$

$$c\text{-}C_2H_4S + h\nu_{193\ nm} \rightarrow HCCH + H_2S \qquad \Delta H_{avai} = 121\ \text{kcal/mol} \quad (III'')$$

$$c\text{-}C_2H_4S + h\nu_{193\ nm} \rightarrow C_2H_3S + H \quad \Delta H_{avai} = \sim 43\ \text{kcal/mol} \quad (IV)$$

Here the heats of formation of *c*-C_2H_4S, $C_2H_4(^1A_g)$, C_2H_4-$(^3B_{1u})$, $S(^3P)$, $S(^1D)$, H_2CCH, HS, H_2CC:, HCCH, H_2S, C_2H_3S, and H are 22.4,[1] 12.54,[6] 76.5,[7] 66.2,[6] 92.7,[8] 71.5,[9] 33.3,,[6] 100.3,[10]

* Corresponding author. E-mail: fqi@lbl.gov.
† Ernest Orlando Lawrence Berkeley National Laboratory.
‡ State University of New York at Stony Brook, and Brookhaven National Laboratory.
§ The Chinese University of Hong Kong.

(1) Felder, P.; Wannenmacher, E. A. J.; Wiedmer, I.; Huber, J. R. *J. Phys. Chem.* **1992**, *96*, 4470.
(2) Kim, H. L.; Satyapal, S.; Brewer, P.; Bersohn, R. *J. Chem. Phys.* **1989**, *91*, 1047.
(3) Chin, W. S.; Chup, B. W.; Mok, C. Y.; Huang, H. H. *J. Chem. Soc., Perkin Trans.* **1994**, *2*, 883.
(4) Tokue, I.; Hiraya, A.; Shobatake, K. *J. Chem. Phys.* **1989**, *91*, 2808.
(5) Carnell, M.; Peyerimhoff, S. D. *Chem. Phys. Lett.* **1993**, *212*, 654.
(6) Chase, M. W., Jr. *J. Phys. Chem. Ref. Data* **1998**, *9*, 1−1951.
(7) Gemein, B.; Peyerimhoff, S. D. *J. Phys. Chem.* **1996**, *100*, 19257.
(8) Moore, C. E. *Atomic Energy Levels*; National Bureau of Standards: Washington, DC, 1952; Vol. I.
(9) Tsang, W. *Heats of Formation of Organic Free Radicals by Kinetic Methods*; Blackie Academic and Professional: London, 1996.
(10) Ahmed, M.; Peterka, D. S.; Suits, A. G. *J. Chem. Phys.* **1999**, *110*, 4248.

10.1021/ja003314v CCC: $20.00
Published on Web 12/08/2000

54.5,[11] −4.9,[6] ∼75,[1] and 52.1 kcal/mol,[6] respectively. ΔH_{avai} is the available energy for a specific channel.

The PTS experiments of Felder and co-workers using electron bombardment ionization for product detection identified channels **I′**, **II**, and **IV** as primary processes in the 193 nm photodissociation of ethylene sulfide, and they inferred a small contribution from the spin-forbidden process **I‴**. We have revisited this system of the UV photodissociation of ethylene sulfide, but with product detection employing soft photoionization by tunable vacuum ultraviolet (VUV) light rather than electron impact ionization. Tunable VUV light as the ionization source in time-of-flight (TOF) measurements has tremendous advantages over the widely used electron bombardment ionization method.[12,13] Tunable VUV ionization can (1) be selective since different molecules can have different ionization potentials, (2) allow for the determination of the relationship between internal energy and ionization cross section, and (3) allow more straightforward detection and analysis of multiple channel processes. Finally, since undulator VUV light is focusable, the ionization region can be much smaller than a comparable electron bombardment ionizer, making both the TOF spectra and angular resolution much higher and background contribution lower. Hence, in this study some additional channels have been identified which were not apparent in the work of Felder and co-workers.[1]

Ethylene, one of photoproducts from *c*-C_2H_4S photodissociation at 193 nm, is a molecule of broad fundamental and practical importance: it is an important combustion intermediate, and it is a synthetic precursor to a vast array of commercial products.[14−18] As the simplest unsaturated system, its electronic structure and spectroscopy have challenged theorists and experimentalists since the early work of Mulliken.[19,20] Despite its importance and the tremendous worldwide production volume, experimental insight into the equilibrium properties of the lowest excited state ($^3B_{1u}$) is lacking. The reason for this can be readily traced to the spin-forbidden transition and the unfavorable Franck−Condon factors between the ground and excited states. The ground electronic state of the molecule is the familiar singlet (^1A_g), planar species (D_{2h}). Promotion of one of the bonding π electrons to an antibonding π^* orbital, with a concomitant change of spin, gives the lowest triplet species ($^3B_{1u}$).[21] The large geometry change accompanying this transition precludes insight into the properties of the $^3B_{1u}$ state near its equilibrium geometry, even for nonoptical probe techniques such as electron scattering that are sensitive to the spin-forbidden transition.[22−24] However, much experimental and theoretical work suggests that photodissociation dynamics studies may be a valuable method for obtaining information about the excited states of polyatomic molecules.[25,26] A possible way to produce triplet ethylene is to prepare the excited states "photochemically" by selecting suitable precursors. Photodissociation may give rise to triplet ethylene directly in the vicinity of its equilibrium geometry. Measurement of the translational energy distributions for a photodissociation event that yields the triplet species can thus be used to obtain important energetic information. A preliminary report on the results for this channel has recently appeared.[21]

Theoretically, Fowler and co-workers reported a mechanistic study of the electrocyclic ring-opening reaction in ethylene sulfide using ab initio molecular orbital theory. The conrotatory process was found to be the favored mechanistic route for ethylene sulfide ring opening.[27] Rohmer and Roos studied the binding mechanism of some cyclic compounds C_2H_4X with X = S, SO, and SO_2 in terms of a donor−acceptor complex between ethylene and the fragment X.[28] The reverse process, S + C_2H_4 → C_2H_4S, is also very interesting. McKee reported a detailed theoretical study of atomic sulfur reactions with alkanes, alkenes, and alkynes using MNDO method. The *c*-C_2H_4S is formed from the S(^{1}D) + C_2H_4 reaction with a small activation barrier (10.6 kcal/mol).[29] Strausz and co-workers also completed a theoretical study of the S + C_2H_4 reaction path using a nonempirical SCF molecular orbital study. While the C_2H_4 + S(^{1}D) reaction was found to be a simple concerted process, the C_2H_4 + S(^{3}P) reaction was identified to be more complicated. The reaction product, the lowest nonvertical $^3\Sigma$ excited state of *c*-C_2H_4S, arises via the sequence: $C_2H_4(^1A_1)$ + S(^{3}P) → C_2H_4S [$^3B_2$] → C_2H_4S [$^3A_2$] → C_2H_4S [$^3\Sigma$]. The ultimate fate of the triplet C_2H_4S is collision-induced intersystem crossing to the ground state.[30]

We report here the use of tunable synchrotron undulator radiation on the Chemical Dynamics Beamline of the Advanced Light Source to probe selectively the singlet and triplet sulfur atom products, as well as other channels of the photodissociation of *c*-C_2H_4S at 193 nm. Also, supporting calculations were performed using the G3 method[31] for the energies of some transition structures and stable species, and using time-dependent B3LYP/6-31G(df) for the excited states. Combining the experimental results with high-level ab initio calculations, the dissociation mechanisms were established.

2. Experimental and Computational Methods

2.1. Experimental Setup. The experiments were performed on beamline 9.0.2.1 of the Advanced Light Source at Berkeley using a rotatable source molecular beam apparatus described in detail elsewhere.[32] Helium was bubbled through a cold (0 °C) ethylene sulfide sample (>98% purity purchased from Aldrich). The total pressure was about 800 Torr, thus yielding a 10% mixture of *c*-C_2H_4S in He. The

(11) Lide, D. R. *Handbook of Chemistry and Physics*; CRC: Boca Raton, FL, 1995−1996; Vol. 75th ed.
(12) Yang, X.; Blank, D. A.; Lin, J.; Heimann, P. A.; Wodtke, A. M.; Lee, Y. T.; Suits, A. G. Chemical Reaction Dynamics Using The Advanced Light Source. In *Synchrotron Radiation Techniques in Industrial, Chemical, and Materials Science*; D'Amico, K. L., Terminello, L. J., Shuh, D. K., Eds.; Plenum Press: New York, 1996; p 119.
(13) Blank, D. A. *Molecular Beam Studies of Unimolecular and Bimolecular Chemical Reaction Dynamics Using VUV Synchrotorn Radiation as a Product Probe*; University of California at Berkeley, 1997.
(14) Gardiner, J. W. C. *Combustion Chemistry*; Springer: New York, 1984.
(15) Robin, M. B. *Higher Excited States of Polyatomic Molecules*; Academic Press: New York, 1985; Vol. III.
(16) Bodke, A. S.; Olschki, D. A.; Schmidt, L. D.; Ranzi, E. *Science* **1999**, *285*, 712.
(17) Pirrung, M. C. *Acc. Chem. Res.* **1999**, *32*, 711.
(18) Younkin, T. R.; Connor, E. F.; Henderson, J. I.; Friedrich, S. K.; Grubbs, R. H.; Bansleben, D. A. *Science* **2000**, *287*, 460.
(19) Wilkinson, P. G.; Mulliken, R. S. *J. Chem. Phys.* **1955**, *23*, 1895.
(20) Merer, A. J.; Mulliken, R. S. *Chem. Rev.* **1969**, *69*, 639.
(21) Qi, F.; Sorkhabi, O.; Suits, A. G. *J. Chem. Phys.* **2000**, *112*, 10707.
(22) Asmis, K. R.; Allan, M. *J. Chem. Phys.* **1997**, *106*, 7044.
(23) Love, D. E.; Jordan, K. D. *Chem. Phys. Lett.* **1995**, *235*, 479.
(24) Wilden, D. G.; Comer, J. *J. Phys. B: At. Mol. Opt. Phys.* **1979**, *12*, L371.
(25) Ashfold, M. N. R.; Baggott, J. E. *Molecular Photodissociation Dynamics*; Royal Society of Chemistry: London, 1977.
(26) Schinke, R. *Photodissociation Dynamics*; Cambridge University Press: Cambridge, 1993.
(27) Fowler, J. E.; Alberts, I. L.; Schaefer, H. F. *J. Am. Chem. Soc.* **1991**, *113*, 4768.
(28) Rohmer, M.-M.; Roos, B. *J. Am. Chem. Soc.* **1973**, *97*, 2025.
(29) McKee, M. *J. Am. Chem. Soc.* **1986**, *108*, 5059.
(30) Strausz, O. P.; Gunning, H. E.; Denes, A. S.; Csizmadia, I. G. *J. Am. Chem. Soc.* **1972**, *94*, 8317.
(31) Curtiss, L. A.; Raghavachari, K.; Redfern, P. C.; Rassolov, V.; Pople, J. A. *J. Chem. Phys.* **1998**, *109*, 7764.
(32) Yang, X.; Lin, J.; Lee, Y. T.; Blank, D. A.; Suits, A. G.; Wodtke, A. M. *Rev. Sci. Instrum.* **1997**, *68*, 3317.

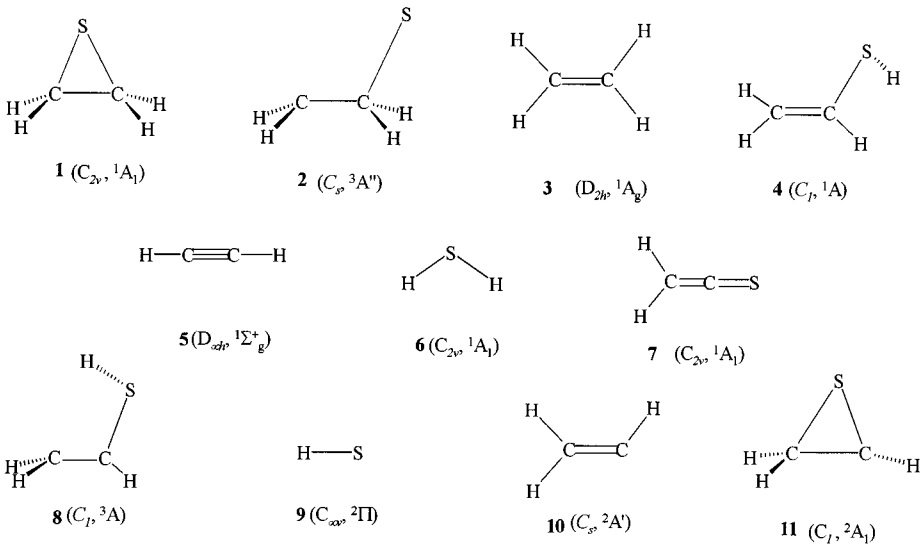

Figure 1. Structural formulas of the various species involved in the dissociations of ethylene sulfide, along with their symmetry point groups and electronic states.

mixture was fed through a pulsed valve (General Valve, series 9) into the main chamber. The nozzle of the valve was heated to ~80 °C to avoid cluster formation. The resulting molecular beam was collimated with two skimmers, and the average molecular beam velocity and speed ratio were measured to be 1310 ± 10 m/s and 10 ± 1, respectively, accomplished via the hole-burning technique at the parent ion mass (m/e = 60). The beam parameters were determined by fitting laser-induced depletion profiles and assuming a number density distribution $f(v) \propto v^2\, e^{-((v/a)-S)^2}$.[33-35]

The molecular beam was intersected at 90° with an ArF excimer laser beam. The laser beam was focused to a 2 × 4 mm^2 spot on the axis of rotation of the molecular beam source and aligned perpendicular to the plane containing the molecular beam and detector axes. Photofragments entering the triply differentially pumped detector region were photoionized using tunable synchrotron radiation, where is 15.2 cm downstream from the photodissociation region. This undulator light source, discussed in detail elsewhere,[36] has a flux of 10^{16} photons/sec (quasi-continuous), an energy bandwidth of 2.2%, and a cross section in the probe region of 0.05 × 0.17 mm^2 (fwhm). A gas filter filled with about 25 Torr Ar was used to eliminate higher harmonics of the undulator radiation.[37] A MgF_2 optical filter also was used to eliminate small contamination of the probe light by higher-energy photons when the probing energy was below 11.0 eV. The photoionized products were mass-selected by a quadrupole mass filter, and the ions were counted with a Daly ion counter. Time-of-flight spectra of the neutral products were measured with a multichannel scaler (MCS) whose bin width (dwell time) was fixed at 1 or 0.5 μs for the measurements reported here. Timing sequences for the laser, pulsed valve, and the MCS were controlled using a digital delay generator. Laser power dependence was measured for all observed channels. Care was taken to ensure that the TOF data were free of multiphoton effects.

The tunability of the VUV light source allowed for the measurements of photoionization efficiency (PIE) spectra and for the selective ionization of products with very low background counts. A series of TOF spectra, recorded at a fixed angle for different photoionization energies, were normalized for the probe photon flux, and integrated to obtain the PIE spectra.

2.2. Computational Methods. The ab initio model of theory employed in this work is the Gaussian-3 (G3) method.[31] In this method, the geometry optimization of a species is carried out at the MP2(full)/6-31G(d) level. In addition, the zero-point vibrational energy correction is also done at this level, with a scaling factor of 0.9661. To calculate the G3 energy of a species, single-point calculations at the levels of QCISD(T)/6-31G(d), MP4/6-31G(d), MP4/6-31+G(d), MP4/6-31G-(2df,p), and MP2(full)/G3large (where G3large is a modified 6-311+G-(3df,2p) basis set), all based on the aforementioned optimized geometry. Once the G3 energy of a species is obtained, the heat of formation at temperature T(ΔH_{fT}) for this species is obtained in the following manner. For molecule ABC, its ΔH_{fT} is calculated from the G3 heat of reaction ΔH_{rT}(AB + C → ABC) and the respective experimental ΔH_{fT} (AB) and ΔH_{fT}(C) for reactants AB and C. This is the method we have employed to obtain the ΔH_{fT} values of a species in its ground state.

In addition, in this work, the transition state structures (**TSs**) of a number of reactions have been identified. The "reactants" and "products" of a given **TS** are confirmed by intrinsic reaction coordinate calculations.

For a species in an excited electronic state, the excitation energy (relative to the ground-state energy) is calculated using the time-dependent (TD)DFT method.[38] In this method the geometry is optimized at the B3LYP/6-31G(df) level.

All of the calculations have been carried out using the Gaussian 98 package of programs.[39] For atomic sulfur, the G3 energy of its ground state (^{3}P) is calculated in the usual way.[31] However, the energy of its excited state ^{1}D apparently cannot be accurately calculated using the Gaussian 98 programs owing to contamination by the (^{1}S) configurations. Hence, to obtain the G3 energy of this state, we simply add the experimental energy difference ΔE(^{1}D − ^{3}P) to the G3 energy of ^{3}P. According to Moore's compilation, ΔE(^{1}D − ^{3}P) for sulfur atom is 25.9 kcal/mol.[8]

Figure 1 shows the structures of the polyatomic species involved in this work, along with their symmetry point groups and electronic states,

(33) Minton, T. K.; Felder, P.; Brudzynski, R. J.; Lee, Y. T. *J. Chem. Phys.* **1984**, *81*, 1759.
(34) Tzeng, W. B.; Yin, H. M.; Leung, W. Y.; Luo, J. Y.; Nourbakhsh, S.; Felsch, G. D.; Ng, C. Y. *J. Chem. Phys.* **1988**, *88*, 1658.
(35) Haas, B.-M.; Minton, T. K.; Felder, P.; Huber, J. R. *J. Phys. Chem.* **1991**, *95*, 5149.
(36) Heimann, P. A.; Koike, M.; Hsu, C. W.; Blank, D.; Yang, X. M.; Suits, A. G.; Lee, Y. T.; Evans, M.; Ng, C. Y.; Flaim, C.; Padmore, H. A. *Rev. Sci. Instrum.* **1997**, *68*, 1945.
(37) Suits, A. G.; Heimann, P.; Yang, X. M.; Evans, M.; Hsu, C. W.; Lu, K. T.; Lee, Y. T.; Kung, A. H. *Rev. Sci. Instrum.* **1995**, *66*, 4841.
(38) Stratmann, R. E.; Scuseria, G. E.; Frisch, M. J. *J. Chem. Phys.* **1998**, *109*, 8218.
(39) Frisch, M. J.; Trucks, G. W.; Schlegel, H. B.; Scuseria, G. E.; Robb, M. A.; Cheeseman, J. R.; Zakrzewski, V. G.; Montgomery, J. A., Jr.; Stratmann, R. E.; Burant, J. C.; Dapprich, S.; Millam, J. M.; Daniels, A. D.; Kudin, K. N.; Strain, M. C.; Farkas, O.; Tomasi, J.; Barone, V.; Cossi, M.; Cammi, R.; Mennucci, B.; Pomelli, C.; Adamo, C.; Clifford, S.; Ochterski, J.; Petersson, G. A.; Ayala, P. Y.; Cui, Q.; Morokuma, K.; Malick, D. K.; Rabuck, A. D.; Raghavachari, K.; Foresman, J. B.; Cioslowski, J.; Ortiz, J. V.; Baboul, A. G.; Stefanov, B. B.; Liu, G.; Liashenko, A.; Piskorz, P.; Komaromi, I.; Gomperts, R.; Martin, R. L.; Fox, D. J.; Keith, T.; Al-Laham, M. A.; Peng, C. Y.; Nanayakkara, A.; Gonzalez, C.; Challacombe, M.; Gill, P. M. W.; Johnson, B.; Chen, W.; Wong, M. W.; Andres, J. L.; Gonzalez, C.; Head-Gordon, M.; Replogle, E. S.; Pople, J. A. *GAUSSIAN 98*, revision A7; Gaussian, Inc.: Pittsburgh, PA, 1998.

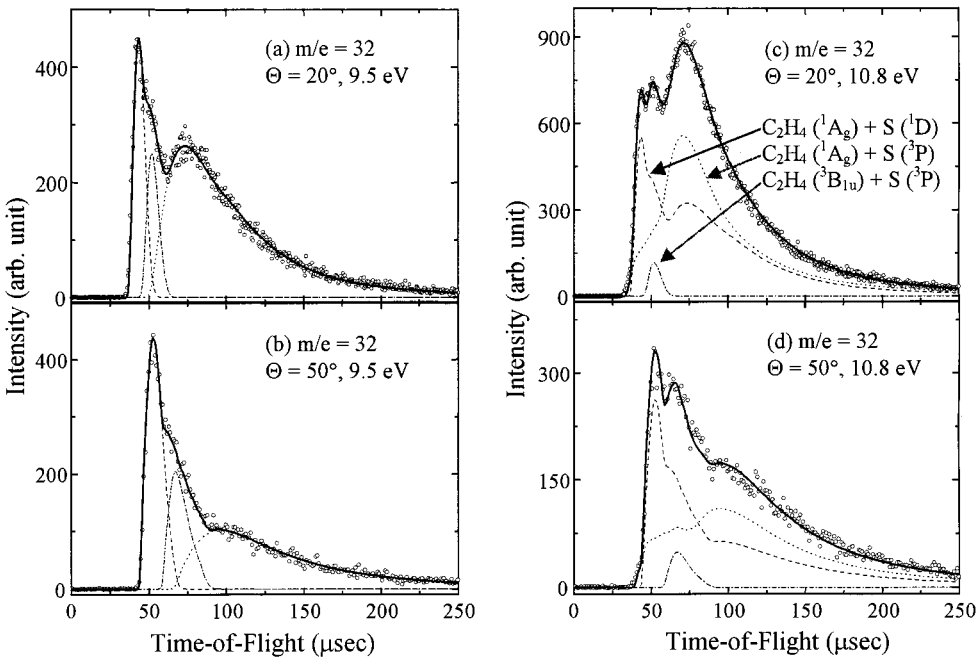

Figure 2. TOF spectra for $m/e = 32$ with 35 mJ/pulse laser energy: (a) 9.5 eV, 20°; (b) 9.5 eV, 50°; (c) 10.8 eV, 20°; and (d) 10.8 eV, 50°. The open circles are the experimental data. The dash lines, the dot lines, and the dash−dot lines are single-channel contributions to the forward convolution fit using the $P(E_T)$s in Figure 3, and the solid lines are the overall fit.

Table 1: G3 Total Energies (E_0), Enthalpies (H_{298}), and Standard Heats of Formation at 0 and 298 K (ΔH^0_{f0} and ΔH^0_{f298}) of Various Species Involved in the Dissociation of Ethylene Sulfide

species	E_0 (hartrees)	H_{298} (hartrees)	ΔH^0_{f0} (kcal/mol)	ΔH^0_{f298} (kcal/mol)
	Equilibrium Structures			
C_2H_4S (**1**)[a]	−476.55949	−476.55521	23.0	20.3
	−476.56296	*−476.55837*	*20.8*	*18.4*
S (^{3}P)	−397.96111			
CH_2CH_2S (**2**)	−476.47639	−476.47093	75.1	73.2
C_2H_4 (**3**)[a]	−78.50601	−78.50200	15.3	13.4
	−78.51298	*−78.50875*	*10.9*	*9.2*
CH_2CHSH (**4**)	−476.49966	−476.49448	60.5	58.4
C_2H_2 (**5**)	−77.27728	−77.27311	54.3	54.5
H_2S (**6**)	−399.23787	−399.23408	−3.5	−4.52
H_2CCS (**7**)	−475.35444	−475.34975	48.0	45.8
CH_2CHSH (**8**)	−476.46328	−476.45748	83.3	81.7
HS (**9**)	−398.59483	−398.59153	34.0	34.1
CH_2CH (**10**)	−77.83308	−77.82091	71.5	75.8
C_2H_3S (**11**)	−475.89880	−475.89452	72.1	69.9
	Transition Structures			
TSa[a]	*−476.42742*	*−476.42164*	*105.8*	*104.2*
TSb	−476.46468	−476.45979	82.5	80.2
TSc	−476.46557	−476.46081	81.9	79.6
TSd	−476.42495	−476.41931	107.4	105.6
TSe	−476.42963	−476.42406	104.5	102.6

[a] The entries given in italic font for these species are G3 energies calculated based on the structures optimized at the MNDO level.

optimized using the above-mentioned method. The calculated G3 energies, enthalpies, and standard heats of formation at 0 and 298 K of all the species involved in the dissociation of *c*-C_2H_4S at 193 nm excitation are listed in Table 1. Considering that the error range for G3 results (for the test suite of molecules) is ±1 kcal/mol,[31] the calculated activation energy should be accurate enough to compare with the experimental results

3. Results

TOF spectra of photofragments from photodissociation of *c*-C_2H_4S at 193 nm have been measured at several angles from 7° to 50°. Signals at $m/e = 59$, 58, 34, 33, 32, 28, 27, and 26 were detected. These correspond to C_2H_3S, C_2H_2S, H_2S, HS, S, C_2H_4, C_2H_3, and C_2H_2 respectively. A forward convolution fit to the data was used to obtain center-of-mass translational energy distributions, $P(E_T)$.[40] In all the TOF spectra presented here, the open circles represent the experimental data, the dash lines, the dot lines, and the dash−dot lines are single-channel contributions to the forward convolution fit, and the solid lines are the overall fit to the data. Specifically, for the TOF spectra of mass 32 with probe photon energy above the IP of S(^{3}P) in this paper, the dash line, the dash−dot line, and the dot line are the single-channel contributions to the forward convolution fits to the process **I′**, **I″** and **I‴**espectively.

3.1. The S + C_2H_4 Channels. The ionization potentials (IP) of the sulfur atom are well-known to be 10.36 and 9.21 eV for the ground state (^{3}P) and the first excited state (^{1}D), respectively.[8] Thus, in this study the S (^{1}D) atom can be selectively ionized by using tunable VUV light at 9.5 eV, whereas contributions from both S (^{3}P) and S (^{1}D) can arise at energy of 10.8 eV.

3.1.a. TOF Spectra of $m/e = 32$ at 9.5 eV Photoionization Energy. Figure 2a and b show TOF spectra of $m/e = 32$ measured at 20° and 50° respectively, by using photoionization energy of 9.5 eV with a MgF_2 optical filter. Two peaks are readily apparent at 43 and 73 μs in the TOF spectrum of Figure 2a: one is sharp and fast, another wide and slow. Less obvious, but nevertheless apparent is a shoulder at 52 μs. Three translational energy distributions (labeled **A**, **B**, and **C**), $P(E_T)$s, shown in Figure 3a were used to fit the TOF data of Figure 2a. $P(E_T)_A$, $P(E_T)_B$, and $P(E_T)_C$ were used to fit the fast part, the middle part, and the slow part of the TOF spectra of Figure 2a, respectively. The larger scattering angle is important for accurate fitting of translational energy distributions to the quickly recoiling photofragments. Thus, the TOF spectrum at 50° (Figure 2b) was measured, and was also fit very well using the same three $P(E_T)$s shown in Figure 3a. These $P(E_T)$s correspond to a channel producing excited-state sulfur (^{1}D) and ground-state ethylene (^1A_g) (Process **I′**), because the photoionization energy used here is below the ionization potential for ground-state

(40) Zhao, X.; Ph.D. Thesis, University of California at Berkeley, 1988.

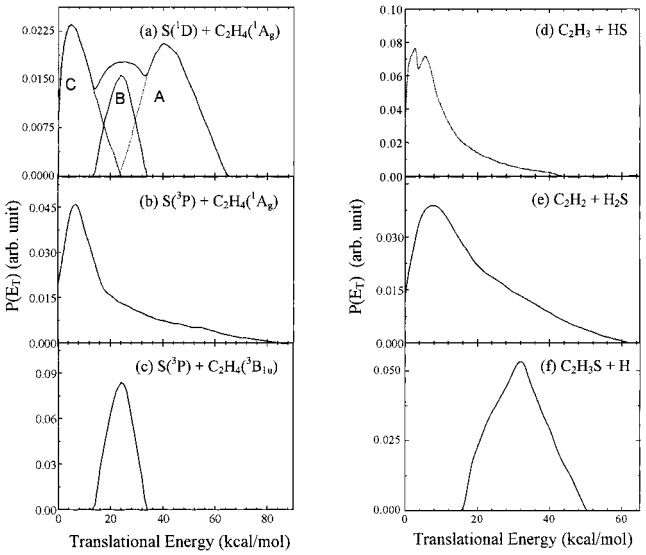

Figure 3. Translational energy distributions, $P(E_T)$s, for the indicated product channels.

sulfur. On the basis of the theoretical calculations and experimental results, three different dissociation mechanisms are suggested to explain the three components in TOF spectra of S in Figure 2a, b, which will be discussed later.

3.1.b. TOF Spectra of *m*/*e* = 32 at 10.8 eV Photoionization Energy. The above measurements were repeated at 10.8 eV and the results are shown in Figure 2c and d. Three peaks are clearly observed in the TOF spectra at the scattering angle of 20°. At this probe energy, both excited S(^{1}D) and ground S(^{3}P) products contribute, but no S atom signal will arise from fragmentation of larger species (C_2H_3S, H_2S and HS), since this is below the onset of dissociative ionization for any of the other fragments. The branching ratio of the three $P(E_T)$s shown in Figure 3a should be constant in fitting the 10.8 eV TOF spectra of $m/e = 32$. Therefore, the three $P(E_T)$s of Figure 3a were combined to one $P(E_T)$, shown as the solid curve of Figure 3a, by using the known intensity and ratio. Two additional translational energy distributions shown in Figure 3b and c were used to fit the 10.8 eV data.

The maximum translational energy of the distribution shown in Figure 3b exceeds the available energy for the S(^{1}D) + C_2H_4(^1A_g) and the S(^{3}P) + C_2H_4($^3B_{1u}$) channels. However, this limit is very close to the available energy for the spin-forbidden S(^{3}P) + C_2H_4(^1A_g) channel. On the other hand, comparing the TOF spectra of mass 32 obtained below and above the IP of the ground-state atom, the *second* peak (~52 μs) of the S atoms actually corresponds partly to the production of ground-state sulfur atoms. These ground state (^{3}P) sulfur atoms are formed at energies near that anticipated for the production of the excited *triplet* state ($^3B_{1u}$) of ethylene (process **I″**). This new channel including excited-state triplet ethylene was not identified in Felder et al.'s study employing electron impact ionization, where it could not have been recognized as a specific feature of the ground-state S atom product. The corresponding translational energy distribution is shown in Figure 3c. Consequently, we assign the $P(E_T)$ of Figure 3c corresponds to the S(^{3}P) + C_2H_4($^3B_{1u}$) channel. Furthermore, TOF spectra of S at 50° and 10.8 eV are also fit very well using the same $P(E_T)$s shown in Figure 3a, b, c.

We ascribe the $P(E_T)$s in Figure 3c and d to different dissociation channels, and thus two $P(E_T)$s were used to fit the S(^{3}P) channels here to derive a best approximation for the heat of formation of the triplet ethylene and branching ratio for the three S atom channels. Actually, these $P(E_T)$s in Figure 3 are overlapped. We should keep in mind that these $P(E_T)$s are not separated clearly, so that the average translational energy for each $P(E_T)$ of Figure 3 derived in this study are somewhat arbitrary. However, this does not affect the assignment of different processes nor the peak positions in each $P(E_T)$.

3.1.c. The Branching Ratio for Processes I′, I″, and I‴. Attempts were made to measure the relative branching between processes **I′**, **I″**, and **I‴**. Branching ratio measurements near the ionization threshold can be misleading, however, since the ionization cross section, σ_i, for S(^{1}D) and S(^{3}P) can be different near their respective onsets and are often perturbed by strong autoionization resonance.[41−43] Previous measurements have shown the photoionization efficiency to be similar for the two states at a probe energy of 15 eV.[44] Thus, measurements of TOF spectra of $m/e = 32$ were made at 15.0 eV photoionization energy and are shown in Figure 4a and b. The three $P(E_T)$s in Figure 3a, b, c fitted these TOF spectra very well. According to this fit, the branching ratio for **I′**, **I″**, and **I‴** is 41:2:57.

We did not give the branching ratio for other channels in this study, since the photoionization cross-section is different for each photoproducts (σ_i) and some radicals' σ_i are still unknown, and we do not feel we can reliably estimate these quantities under the conditions of the experiment.

3.1.d. TOF Spectra of *m*/*e* = 28. Figure 4c, d show the TOF spectra of $m/e = 28$, the momentum matched partner of $m/e = 32$, at the scattering angle of 20° with photon energies of 11.0 and 10.0 eV, respectively. The TOF spectra of $m/e = 28$ were fitted very well using the $P(E_T)$s shown in Figure 3a, b, c, with some adjustment of their relative contributions, consistent with the anticipated dependence of the photoionization cross section on internal energy in the product. Indeed, we can get some insight into this by examining the behavior of the TOF spectra as a function of probe photon energy. The ionization potential of ethylene is well-known to be 10.51 eV.[11] Comparing the TOF spectra of $m/e = 28$ recorded above and below the IP of C_2H_4, an evident change occurred in the fast part. This means the "cold" ethylene cannot be ionized at the photon energy of 10.0 eV. The second peak becomes clearer, which confirms the presence of considerable internal energy.

3.1.e. TOF Spectra of S at Lower Laser Power. Felder et al.[1] assigned the multiple peaks in their TOF distribution to multiphoton process induced by their photolysis laser. If this were a case, C_2H_3S and HS could absorb another 193 nm photon and dissociate to S. Actually, it is hard to discern any difference from the TOF spectrum of $m/e = 32$ between using low power and high power.[1] To avoid the multiphoton processes, we carefully checked the laser power dependence for all observed channels. Figure 5 shows the TOF spectra of S using different laser powers. No significant change was observed in the TOF spectra of S when the laser power was used at 0.5 mJ/pulse (6.2 mJ/cm^2). One possible explanation for the difference here is that electron impact ionization was used in Felder and coworkers' study, and hence the larger photofragments could dissociatively ionize to smaller fragments. Certainly for the S atom products in our study we can neglect this possibility.

3.2. The HS + C_2H_3 Channel. Figure 6 shows TOF spectra of $m/e = 27$ and 33 measured at the indicated scattering angles and photon energies, which correspond to a channel producing

(41) Gibson, S. T.; Greene, J. P.; Ruscic, B.; Berkowitz, J. *J. Phys. B: At. Mol. Opt. Phys.* **1986**, *19*, 2825.
(42) Pratt, S. T. *Phys. Rev. A* **1988**, *38*, 1270.
(43) Chen, C. T.; Robicheaux, F. *Phys. Rev. A* **1994**, *50*, 3968.
(44) McGivern, W. S.; Sorkhabi, O.; Rizvi, A. H.; Suits, A. G.; North, S. W. *J. Chem. Phys.* **2000**, *112*, 5301.

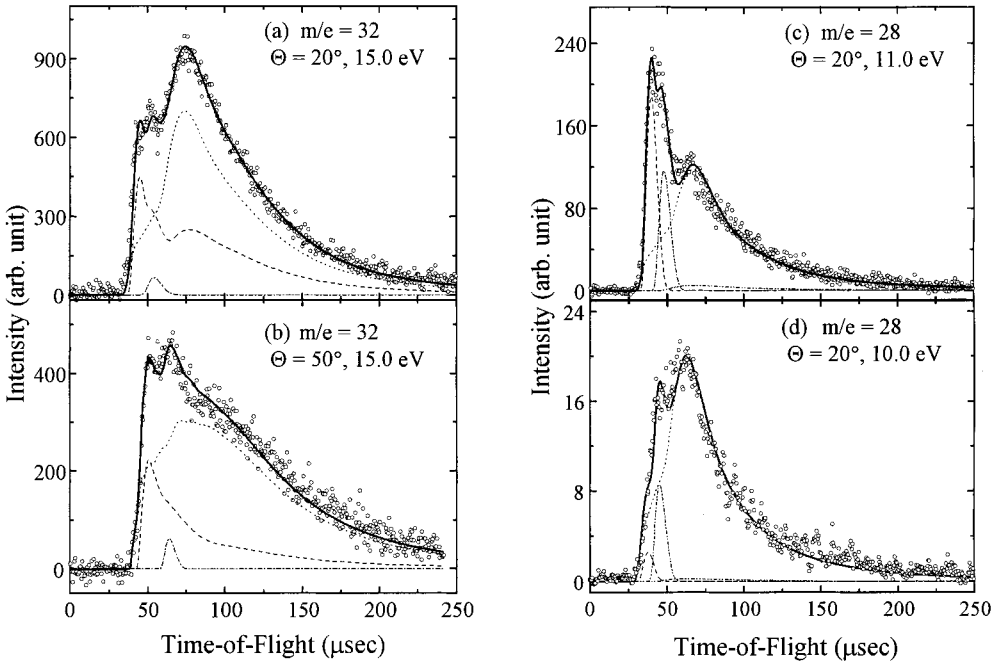

Figure 4. TOF spectra for $m/e = 32$ and 28 with 35 mJ/pulse laser energy: (a) $m/e = 32$, 20°, 15.0 eV; (b) $m/e = 32$, 50°, 15.0 eV; (c) $m/e = 28$, 20°, 11.0 eV; (d) $m/e = 28$, 20°, 10.0 eV. The open circles are the experimental data. The dash lines, the dot lines, and the dash−dot lines are single-channel contributions to the forward convolution fit using the $P(E_T)$s in Figure 3, and the solid lines are the overall fit.

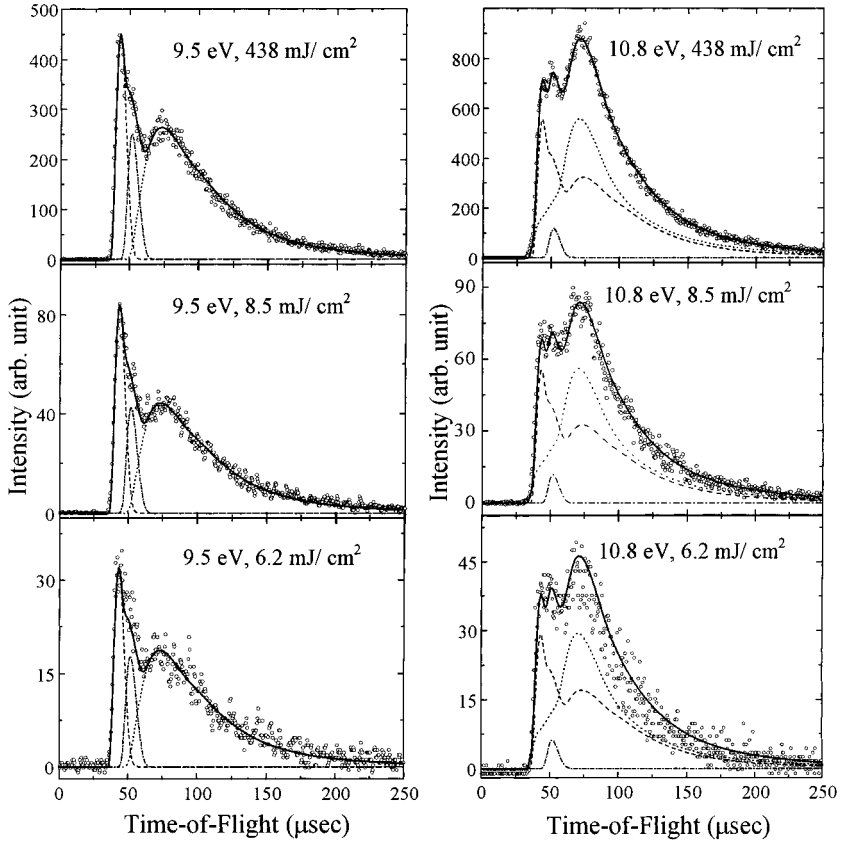

Figure 5. TOF spectra of $m/e = 32$ at the scattering angle of 20° with indicated probe photon energy and laser powers.

the C_2H_3 and HS radicals (process **II**). Two peaks are observed in TOF spectra of $m/e = 33$. A translational energy distribution shown in Figure 3d was used to fit TOF spectra of $m/e = 27$ and 33. This translational energy distribution has a peak at 2.7 and 5.5 kcal/mol respectively, and extends to about 43 kcal/mol with an average translational energy release of 12 kcal/mol. Our $P(E_T)$ is similar to the previous report,[1] although, a bimodal distribution was more clearly observed in our high-resolution study.

3.3. The $H_2S + C_2H_2$ Channel. Figure 7 shows TOF spectra of mass 26 and 34 measured at 20° and 40° with indicated photoionization energies. TOF spectra of $m/e = 34$ were fitted using a translational energy distribution shown in Figure 3e. A channel representing the production of H_2S with C_2H_2, is

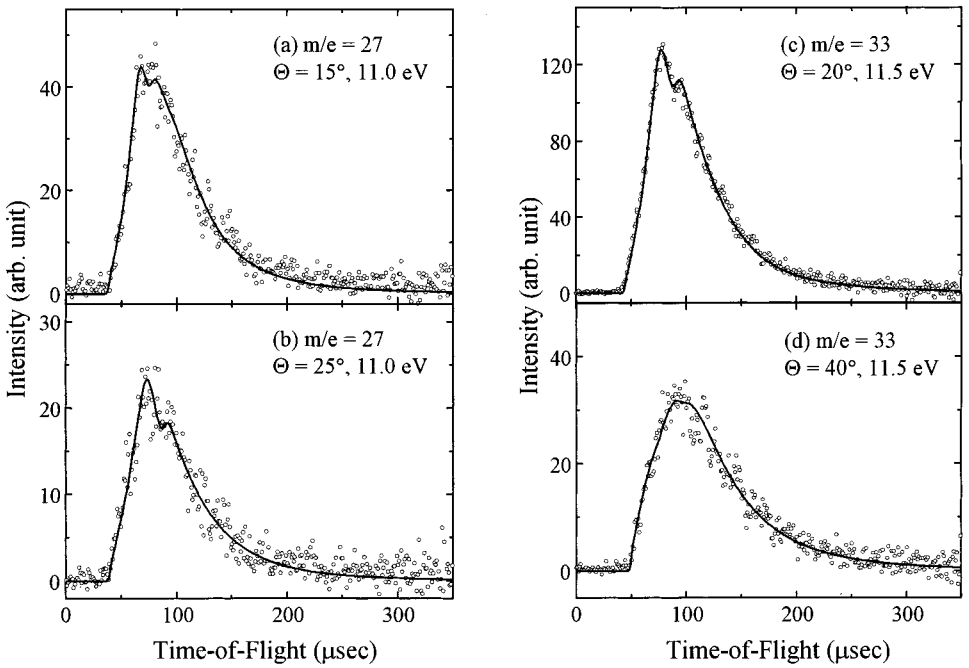

Figure 6. TOF spectra for $m/e = 27$ and 33 with the indicated photoionization energies and scattering angles. The circles are the experimental data, and the solid lines are the forward convolution fits using the $P(E_T)$ in Figure 3d.

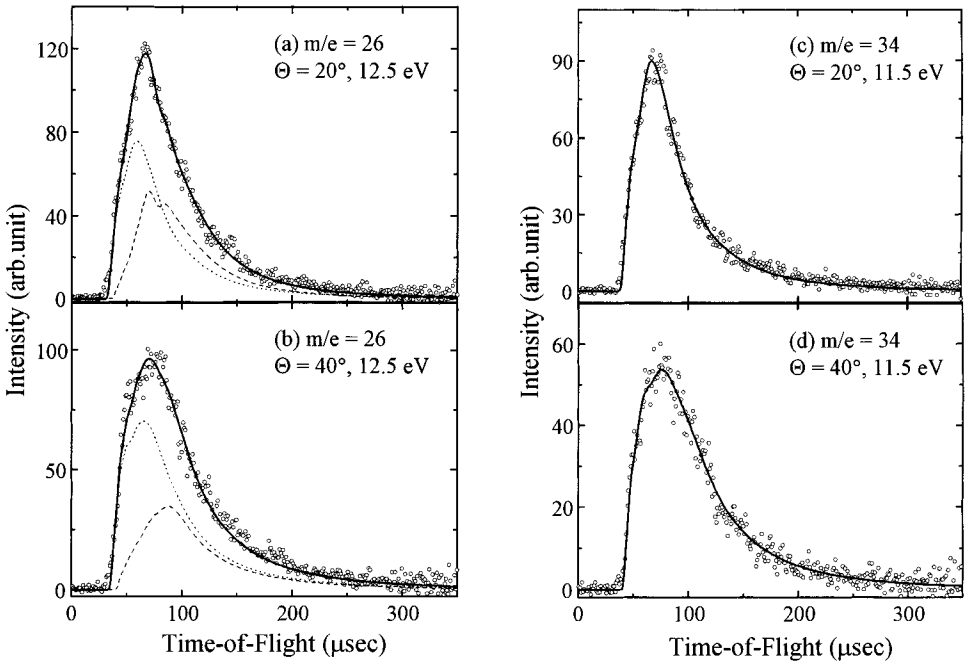

Figure 7. TOF spectra for $m/e = 26$ and 34 with the indicated photoionization energies and scattering angles. The circles are the experimental data. The dot lines and the dash lines are the forward convolution fits using the $P(E_T)$s in Figure 3e and d.

observed at 193 nm photodissociation of *c*-C_2H_4S in this study (process **III″**). However, TOF spectra of $m/e = 26$ were fitted using two translational energy distributions: one from momentum-matched fragment channel $H_2S + C_2H_2$, and another one from dissociative ionization of larger unstable radical C_2H_3 at the 12.5 eV probe energy. The assignment of the $m/e = 34$ fragment at 11.5 eV (literature value for the IE of H_2S is 10.5 eV) is unambiguous, however, and the TOF spectra momentum match to the fast portion of the $m/e = 26$ data. An average translational energy of 21.3 kcal/mol was obtained for this channel with the translational energy extending out to 63 kcal/mol. An exit barrier of roughly 7.6 kcal/mol was observed for this channel. The signal of mass 26 was found to be much stronger than that of mass 27.

3.4. The H Atom Elimination Channel. H atom elimination channel was observed in our study on the (parent-1) mass. The TOF spectrum of C_2H_3S at 10° is shown in Figure 8a, which was fitted using a translational energy distribution, $P(E_T)$, shown in Figure 3f. A photon energy of 10.5 eV with a MgF_2 filter was used to ionize the C_2H_3S fragment. This $P(E_T)$ peaks at 28 kcal/mol, extends to 48 kcal/mol with an average translational energy release of 28.8 kcal/mol. However, Felder and co-workers measured this channel by recording TOF spectra of $m/e = 1$. Three components were observed in their TOF spectra of $m/e = 1$. This is evidently because of high laser power and electron impact ionization employed in their work. The complicated TOF spectra of $m/e = 1$ precluded the data fit. Here we measured $m/e = 59$ (C_2H_3S) signal using VUV photoion-

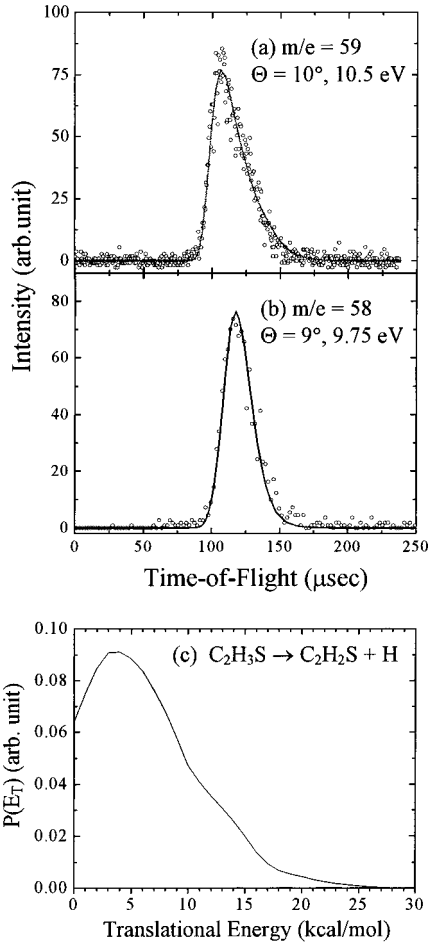

Figure 8. (a) TOF spectra for $m/e = 59$ at a scattering angle of 10° and a photoionization energy of 10.5 eV. The circles are the experimental data, and the solid lines are the forward convolution fits using the $P(E_T)$ in Figure 3f. (b) TOF spectra for $m/e = 58$ at a scattering angle of 9° and a photoionization energy of 9.75 eV. The circles are the experimental data and the solid lines are the forward convolution fits using the $P(E_T)$ in (c). (c) Translational energy distribution $P(E_T)$ for the secondary dissociation of C_2H_3S used to fit TOF spectra of (b).

ization. Hence, the translational energy distribution derived from this work directly reflects the energy distribution of H atom elimination process, if assuming no secondary dissociation from C_2H_3S.

4. Discussion

Figure 9 shows schematically two types of unimolecular dissociation potential curves and the resulting relative translational energy distributions.[45] Neglecting the case of impulsive dissociation for the moment, if the unimolecular reaction does not have a barrier for the reverse recombination reaction (Figure 9a), the energy distributions at the transition state may be used to predict those for the products. If there is a barrier for recombination of reaction products, as Figure 9b, the product energy distributions are usually nonstatistical and different from those at the transition state. This is because the potential energy released in going from the transition state to products is channeled nonstatistically to translation, vibration, and rotation. For reaction ABC → [Transition State (TS)] → AB + C, the reaction barrier (E_{rxnbr}, or call activation barrier) and the exit barrier (E_{exitbr}, or call reverse barrier) are defined as following equations:

(45) Steinfeld, J. I.; Francisco, J. S.; Hase, W. L. *Chemical Kinetics and Dynamics*; Prentice Hall: New Jersey, 1998.

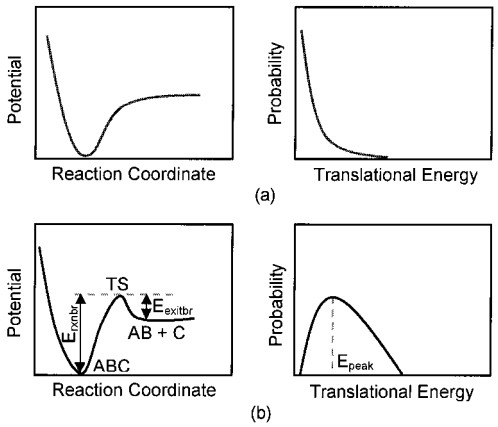

Figure 9. Relationship between the reaction path potential energy curve for a unimolecular dissociation reaction and the translational energy distribution of the dissociation products: (a) the unimolecular reaction does not have a barrier for the reverse recombination reaction; (b) the reaction has a barrier for the reverse recombination reaction.

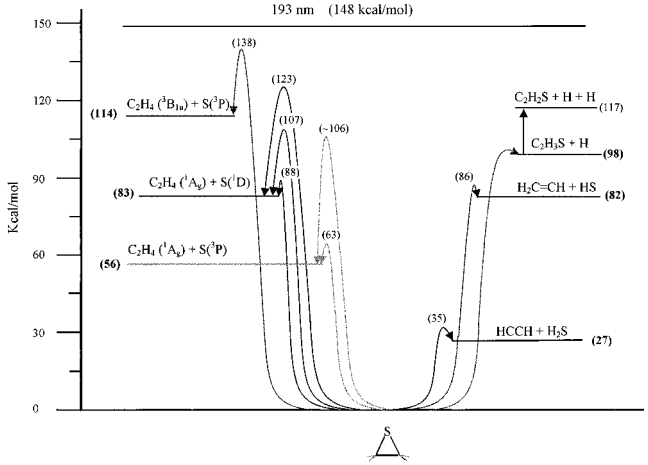

Figure 10. Energy diagram showing all observed product channels from 193 nm dissociation of ethylene sulfide, along with exit barriers estimated roughly from our experimental results.

$$\Delta H_{rxn} = \Delta H^0_f(AB) + \Delta H^0_f(C) - \Delta H^0_f(ABC) \quad (1)$$

$$E_{rxnbr} = \Delta H_{rxn} + E_{exitbr} = \Delta H^0_f(TS) - \Delta H^0_f(ABC) \quad (2)$$

$$E_{exitbr} = E_{peak} = \Delta H^0_f(TS) - [\Delta H^0_f(AB) + \Delta H^0_f(C)] \quad (3)$$

Here, ΔH^0_f and ΔH_{rxn} are heat of formation and reaction energy, respectively. E_{peak} is the translational energy relating to the peak position in the translational energy distribution, which can be derived from our translational energy distributions (see Figure 9b). Hence, the exit barrier can be derived roughly from our translational energy distributions. In fact, the dissociation process is considerably more complex than this simple model. Hence, we should keep in mind that the reaction barrier or the exit barrier derived from the experiments in this paper is at best approximate. Indeed, in the $m/e = 26$ case below, we find this picture fails completely. Nevertheless, it provides a useful basis to compare qualitatively the value from our experiment to results of theoretical calculations.

The energy diagram of Figure 10 shows all observed product channels from 193 nm dissociation of ethylene sulfide, along with reaction barriers estimated roughly from our $P(E_T)$s. Table

Table 2. Energy Partition of Different Dissociation Channels of Ethylene Sulfide at 193 nm Excitation (kcal/mol)

dissociation channel		total available E_{tot}	max $E_{max-tran}$	av energy $\langle E_{tran}\rangle$	av energy $\langle E_{int}\rangle$	$\langle E_{tran}\rangle/\langle E_{int}\rangle$	exit barrier
	$P(E_T)_A$	65	65	42.8	22.2	66/34	40.2
I′	$P(E_T)_B$	65	34	23.7	41.3	36/64	24.1
	$P(E_T)_C$	65	24	8.7	56.3	13/87	4.9
I″		~34[a]	34	23.7	10.3	70/30	24.2
I‴		92	85	19.9	72.1	22/78	6.7
II		66	43	12.0	54.0	18/82	2.7, 5.5
III		121	63	21.3	99.7	18/82	7.6
IV		~48[a]	48	28.8	19.2	60/40	28.0

[a] Here we used the heats of formation of $C_2H_4(^3B_{1u})$ and C_2H_3S according to our PTS results.

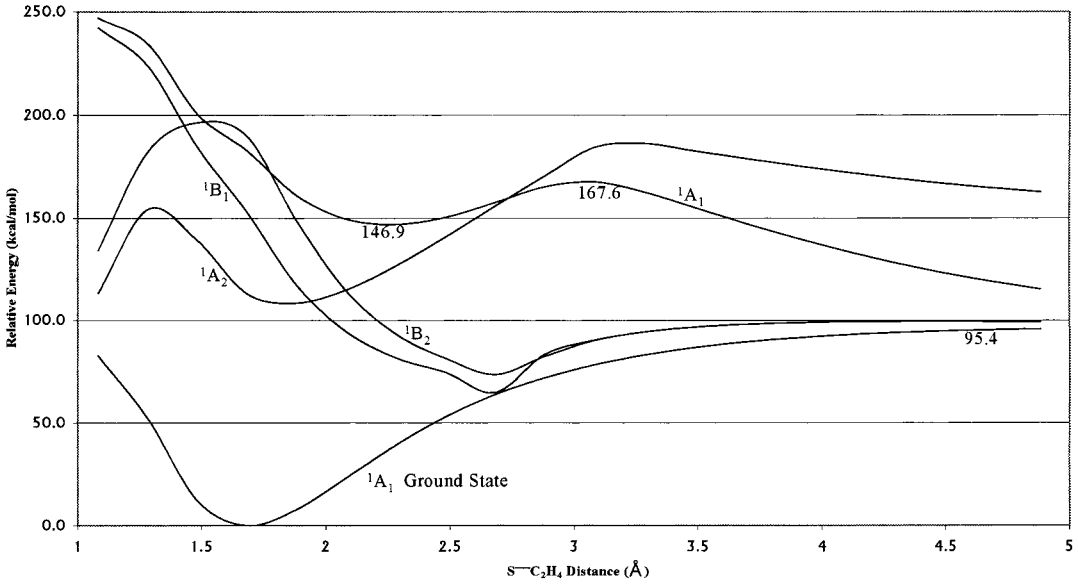

Figure 11. Singlet potential energy profiles for dissociation $C_2H_4S \rightarrow C_2H_4(^1A_g) + S(^1D)$, maintaining C_{2v} symmetry throughout.

2 lists the energetic information for all observed channels, including the maximum translational energy in each distribution ($E_{max-tran}$), the average translational energy ($\langle E_{tran}\rangle$), the average internal energy ($\langle E_{int}\rangle$), the ratio $\langle E_{tran}\rangle/\langle E_{int}\rangle$, and the exit barrier relative to reaction products.

4.1. The S + C_2H_4 Channel. 4.1.a. The S(^{1}D) + $C_2H_4(^1A_g)$ Channel. The three translational energy distributions shown in Figure 3a correspond to a channel forming $S(^1D) + C_2H_4(^1A_g)$. The average translational energy is 42.8, 23.7, and 8.7 kcal/mol for the fast $P(E_T)$, the middle $P(E_T)$, and the slow $P(E_T)$, respectively. The maximum translational energy in each distribution is derived to be 65, 34, and 24 kcal/mol respectively for the three components mentioned above. In each case the available energy is 65 kcal/mol. Our $P(E_T)$ indicates three exit barriers of roughly 4.9, 24.1, and 40.2 kcal/mol.

The question, then, is the nature of the dynamics underlying these distinct distributions. The initially excited Rydberg state of *c*-C_2H_4S is expected to have predominantly singlet character,[4] and the products are all singlets, and thus for these channels we confine our discussion to the singlet surfaces. First, we discuss the formation mechanism associated with $P(E_T)_A$ of Figure 3a. Figure 11 shows the singlet potential energy profiles for ethylene sulfide dissociation in C_{2v} symmetry as a function of the S−C_2H_4 distance, obtained using the time-dependent (TD)DFT method. The dissociation corresponding to $P(E_T)_A$ is likely to occur directly on the initially excited $^1A_1$ state, giving rise to the greatest translational energy release. Furthermore, another dissociation process, corresponding to $P(E_T)_B$, is likely to start with the excited $^1A_1$ state, then dissociation occurs after internal conversion to the $^1B_2$ surface. Although this coupling vanishes in a strict C_{2v} symmetry, in the C_s symmetry space in which the dissociation actually occurs, this coupling can be significant. This pathway gives a calculated heat of reaction equal to 95.4 kcal/mol, whereas, the experimental heat of reaction is 83 kcal/mol for the $C_2H_4(^1A_g) + S(^1D)$ channel. A possible source of the difference is that the singlet electronic state of the S atom described by the Gaussian-98 program is a mixture of ^{1}D and ^{1}S, instead of a pure ^{1}D. Furthermore, it is not surprising that the calculated potential energy surfaces are higher than the experimental excitation energy of 148 kcal/mol (193 nm) because the calculated singlet potential profiles were derived by changing only one coordinate, the C−S distance, and maintaining the C_{2v} symmetry. In fact the excited states of *c*-C_2H_4S are ring distorted equilibrium conformations. Finally, the lowest energy peak in the S(^{1}D) distribution is likely to arise from internal conversion from the aforementioned states to the ground state. Figure 12a shows the potential energy surface for dissociation *c*-$C_2H_4S \rightarrow C_2H_4(^1A_g) + S(^1D)$ through a transition structure **TSa** with an activation barrier of 85.1 kcal/mol. Here C_{2v} symmetry is enforced throughout, and the G3 energies of all three species involved in this surface are calculated on the basis of structures optimized at the MNDO level. The experimental activation energy is around 88 ± 1 kcal/mol, which is in good agreement with the theoretical calculation. The $^1B_1$ and $^1A_2$ surfaces shown in Figure 11 are not likely to play a role, since even in C_s symmetry, they become A″, so that coupling to A′ states is negligible. Imaging experiments show significant anisotropy in the S(^{1}D) products, confirming this picture of rapid dissociation.[46]

(46) Qi, F.; Ahmed, M.; Peterka, D. S.; Sorkhabi, O.; Suits, A. G., unpublished results.

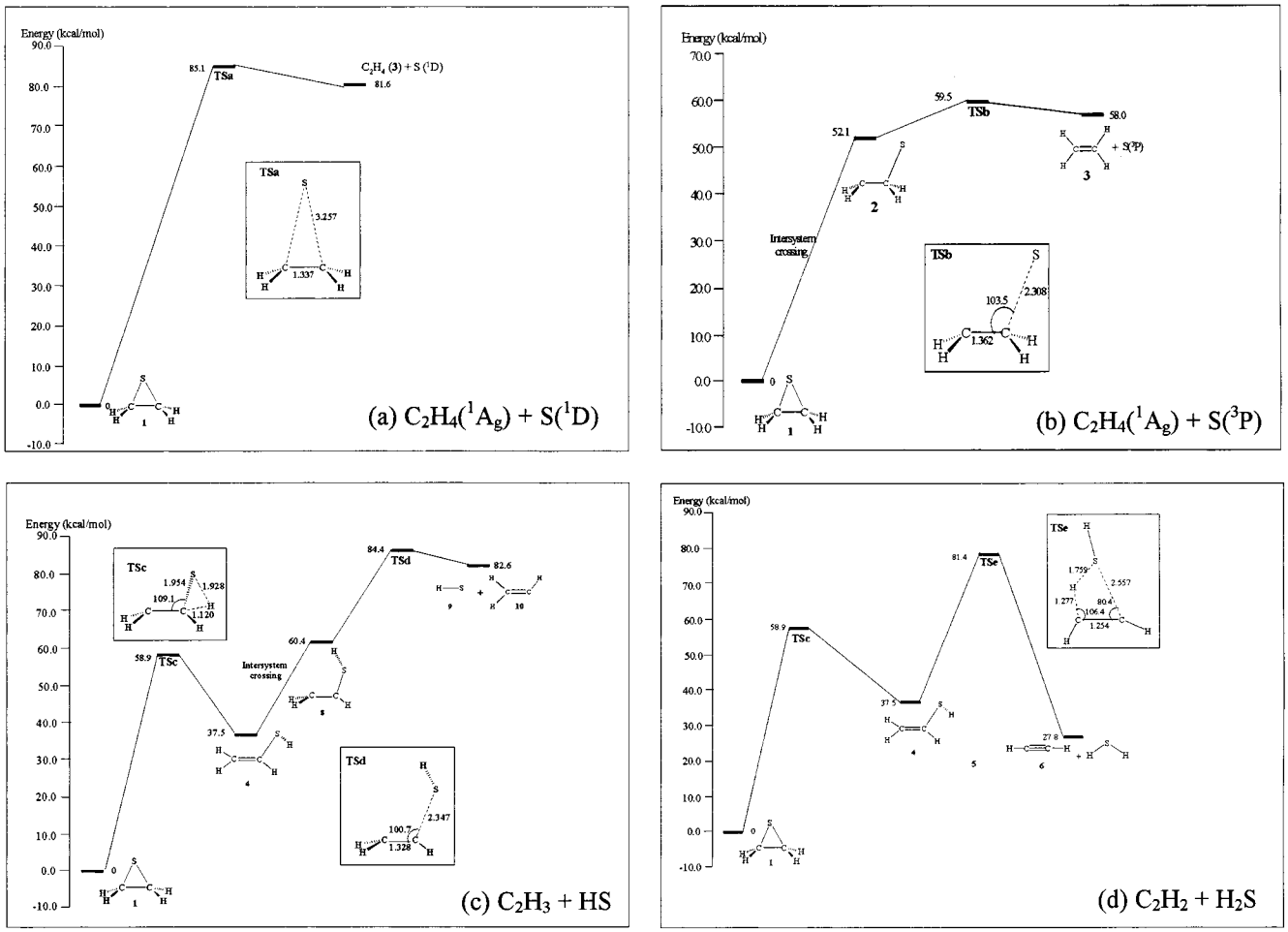

Figure 12. Potential energy surface showing the possible mechanism for indicated dissociation channel: (a) $C_2H_4S \rightarrow C_2H_4(^1A_g) + S(^1D)$; (b) $C_2H_4S \rightarrow C_2H_4(^1A_g) + S(^3P)$. Note that **2** and **TSb** are triplet species; (c) $C_2H_4S \rightarrow C_2H_3(^2A') + HS$. Note that **8** and **TSd** are triplet species; (d) $C_2H_4S \rightarrow C_2H_2\ (^1A_1) + H_2S$

4.1.b. The $S(^3P) + C_2H_4\ (^1A_g)$ Channel. The channel representing the production of $S(^3P)$ and $C_2H_4(^1A_g)$ has an average translational energy of 20 kcal/mol, extending out to about 85 kcal/mol with an estimated exit barrier of roughly 6.7 kcal/mol. The maximum translational energy is close to available energy of 92 kcal/mol. The occurrence of this spin-forbidden channel is not too surprising because the heavy S atom increases the probability of intersystem crossing. Ground-state ethylene sulfide has C_{2v} symmetry. Adopting the convention that *z* corresponds to the C_2 axis and that the ring lies in the *yz* plane, the ground-state electronic configuration may be written as:

$$...(2b_1)^2(7a_1)^2(1a_2)^2(8a_1)^2(4b_2)^2(3b_1)^2;\ \tilde{X}\ ^1A_1$$

where its outermost $3b_1$ orbital is almost nonbonding and its main component is the $3p_x$ orbital of the sulfur atom (93%).[4,47] Moreover, abundant formation of spin-forbidden fragment pairs have been observed in other sulfur-containing compounds such as CS_2, SO_2 and thiophene.[48−50] If we look at the $P(E_T)$ of Figure 3b in detail, it looks like two $P(E_T)$s overlap: one is very broad, another one very narrow with a peak at around 6.7 kcal/mol. This spin-forbidden dissociation could proceed via different mechanism on two surfaces.

To dissociate into $S(^3P)$ and $C_2H_4(^1A_g)$, *c*-C_2H_4S must first undergo an intersystem crossing and ring-opening reaction to form biradical **2**. The radical **2** then forms the products $S(^3P)$ and $C_2H_4(^1A_g)$ via **TSb**. The schematic energy profile of this process and the structure of **TSb** are shown in Figure 12b. The G3 barrier of this stepwise reaction is 59.5 kcal/mol, in fair agreement with the experimental result (63 ± 2 kcal/mol). This small exit barrier (1.5 kcal/mol, see Figure 12b) is also in good agreement with the previous report: a reaction barrier of ground-state sulfur atom with ethylene was measured to be 1.58 kcal/mol.[51] This stepwise process likely occurs on the $^3B_2$ electronic state following intersystem crossing.

On the other hand, the other dissociation is likely to begin with excitation of the singlet $^1A_1$ state, followed by an intersystem crossing to the triplet state $^3B_2$. Figure 13 shows the triplet potential energy profiles for dissociation $C_2H_4S \rightarrow C_2H_4(^1A_g) + S(^3P)$. These maintain the C_{2v} symmetry throughout, including the potential energy profile of the $^1A_1$ state. As we mentioned above, the theoretical value was overestimated. We should keep in mind that C_{2v} geometry may have little to do with the actual dissociation event but provides a starting point for discussion. The complicated intersystem crossing is also reflected in the $P(E_T)$ of Figure 3b, in which the translation energy distribution beyond ∼20 kcal/mol becomes flat.

(47) Morgan, R. A.; Puyuelo, P.; Howe, D.; Ashfold, M. N. R.; Buma, W. J.; Milan, J. B.; de Lange, C. A. *J. Chem. Soc., Faraday Trans.* **1994**, *90*, 3591.

(48) Waller, I. M.; Hepburn, J. W. *J. Chem. Phys.* **1987**, *87*, 3261.

(49) Effenhauser, C. S.; Felder, P.; Huber, J. R. *Chem. Phys.* **1990**, *142*, 311.

(50) Qi, F.; Sorkhabi, O.; Rizvi, A. H.; Suits, A. G. *J. Phys. Chem. A* **1999**, *103*, 8351.

(51) Davis, D. D.; Klemm, R. B.; Braun, W.; Pilling, M. *Int. J. Chem. Kinet.* **1972**, *4*, 383.

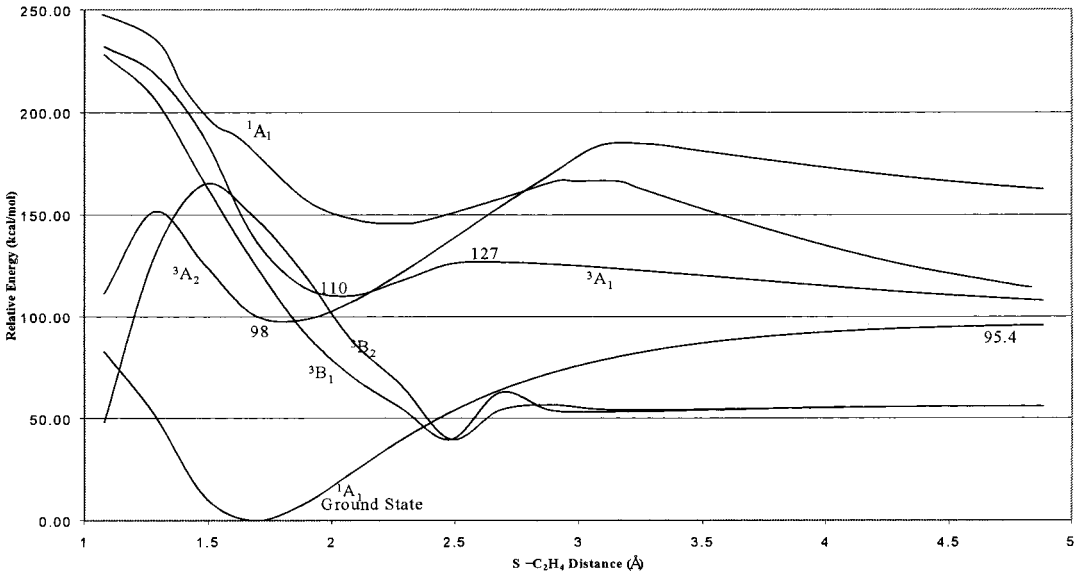

Figure 13. Triplet potential energy profiles for dissociation $C_2H_4S \rightarrow C_2H_4(^1A_g) + S(^3P)$, maintaining C_{2v} symmetry throughout, also with the $^1A_1$ state.

In Felder and co-workers' PTS study, only production of ground-state C_2H_4 was reported, and four contributions to the sulfur atom signal were observed, including HS and C_2H_3S dissociative ionization. Average translation energies for the $S(^1D) + C_2H_4$ (^1A_g) fragments of 32 ± 2 and 20.5 ± 4.5 kcal/mol have been obtained by different groups.[1,2]

The probing technique employed in Kim et al.'s study was specific to nascent S atoms and thus to the dissociation process yielding C_2H_4 + S. They probed for the three lowest electronic states, $S(^3P)$, $S(^1D)$, and $S(^1S)$, but found evidence only for the formation of sulfur in the ^1D state. In Felder et al.'s study, a small portion of the $P(E_T)$ distribution was asssigned to the formation of the ground-state sulfur + ethylene fragment pair, the relative contributions of the $S(^1D) + C_2H_4(^1A_g)$ and $S(^3P) + C_2H_4(^1A_g)$ channels were approximately 1 and 0.05, respectively. In Felder and co-workers' study,[1] translational energy distribution of $S + C_2H_4$ beyond 64 kcal/mol, which is the limit of the $S(^1D) + C_2H_4(^1A_g)$ channel, were unambiguously assigned to $S(^3P) + C_2H_4(^1A_g)$, while these below this limit were all assigned to **I′**. Their assignment does not reflect the real translational energy distribution. Our result shows the branching ratio of 41:2:57 for the three different channels mentioned above. It is not clear why Kim et al.[2] failed to see the contribution of ground state S atoms implied both in Felder's work and in ours. The relative sensitivity of their probe methods to the excited and ground state S atoms appears to be the most likely explanation for the discrepancy.

4.1.c. The $S(^3P) + C_2H_4(^3B_{1u})$ Channel and Triplet Ethylene C_2H_4 ($^3B_{1u}$). Finally, we discuss the *triplet* ethylene channel. The production of $S(^3P)$ plus $C_2H_4(^3B_{1u})$ is also consistent with a process occurring on a singlet electronic surface. The maximum translational energy of the $S(^3P) + C_2H_4(^3B_{1u})$ channel is 34 kcal/mol with an average translational energy of 23.7 kcal/mol. The $P(E_T)$ in Figure 3c indicates an exit barrier of roughly 24 kcal/mol for this channel. These products are very fast compared to the available energy of this channel. This is a direct dissociation process occurring on the singlet excited potential energy surface without internal conversion. Hence, the triplet ethylene can be formed at near its equilibrium geometry, in which the two CH_2 groups are believed to lie in perpendicular planes. Thus, we can derive an estimate, actually an upper limit, for the heat of formation for triplet ethylene. We should note that the assignment of the intermediate peak in the triplet S product to triplet ethylene is by no means definitive. Other possible explanations include internal conversion with dissociation on a different potential surface, as invoked for the $S(^1D)$ product. It might be tempting to associate this peak with a similar peak in the $S(^1D)$ distribution. A moment's consideration reveals, however, owing to the different electronic energy in the products, it cannot be related to the middle peak in the $S(^1D)$ distribution. We believe, in fact that this peak in the $S(^3P)$ distribution is related to the *fastest* peak in the $S(^1D)$ distribution, that is, it arises from direct dissociation on the initially prepared singlet surface. Although the evidence presented here for the production of triplet ethylene from ethylene sulfide photodissociation is by no means definitive, we believe this is the most likely explanation for the observations.

Some indirect support for this assignment may be found in recent work on a related molecule, ethylene episulfoxide (C_2H_4SO), by Weiner and co-workers.[52] They used time-resolved laser-induced fluorescence spectroscopy to probe the SO ($X^3\Sigma^-$) photofragment on the ($B^3\Sigma^- - X^3\Sigma^-$) transition.[52] Two physical models, Franck−Condon and impulsive, were used to model the distribution of internal energy in the SO ($X^3\Sigma^-$) photofragment from 193 and 248 nm photodissociation of C_2H_4SO. Both models demonstrated that a reasonable fit to the experimental data was obtained only when the ethylene is triplet state ($^3B_{1u}$), not ground state. Furthermore, they suggested that the photodissociation of C_2H_4SO, at both 193 and 248 nm, proceeded via a concerted bond cleavage process.

Ethylene has been the subject of many ab initio theoretical and experimental studies.[7,22−24,53−59] Here, we derive the heat

(52) Wu, F.; Chen, X.; Weiner, B. R. *J. Am. Chem. Soc.* **1996**, *118*, 8417.
(53) Wiberg, K. B.; Hadad, C. M.; Forseman, J. B.; Chupka, W. A. *J. Phys. Chem.* **1992**, *96*, 10756.
(54) Foresman, J. B.; Head-Gordon, M.; Pople, J. A.; Frisch, M. J. *J. Phys. Chem.* **1992**, *96*, 135.
(55) Danovich, D.; Marian, C. M.; Neuheuser, T.; Peyerimhoff, S. D.; Shaik, S. *J. Phys. Chem. A* **1998**, *102*, 5923.
(56) Walker, I. C.; Stamatovic, A.; Wong, S. F. *J. Chem. Phys.* **1978**, *69*, 5532.
(57) Sension, R. J.; Mayne, L.; Hudson, B. *J. Am. Chem. Soc.* **1987**, *109*, 5036.
(58) Sension, R. J.; Hudson, B. S. *J. Chem. Phys.* **1989**, *90*, 1377.
(59) Lin, J. J.; Hwang, D. W.; Lee, Y. T.; Yang, X. *J. Chem. Phys* **1998**, *109*, 2979.

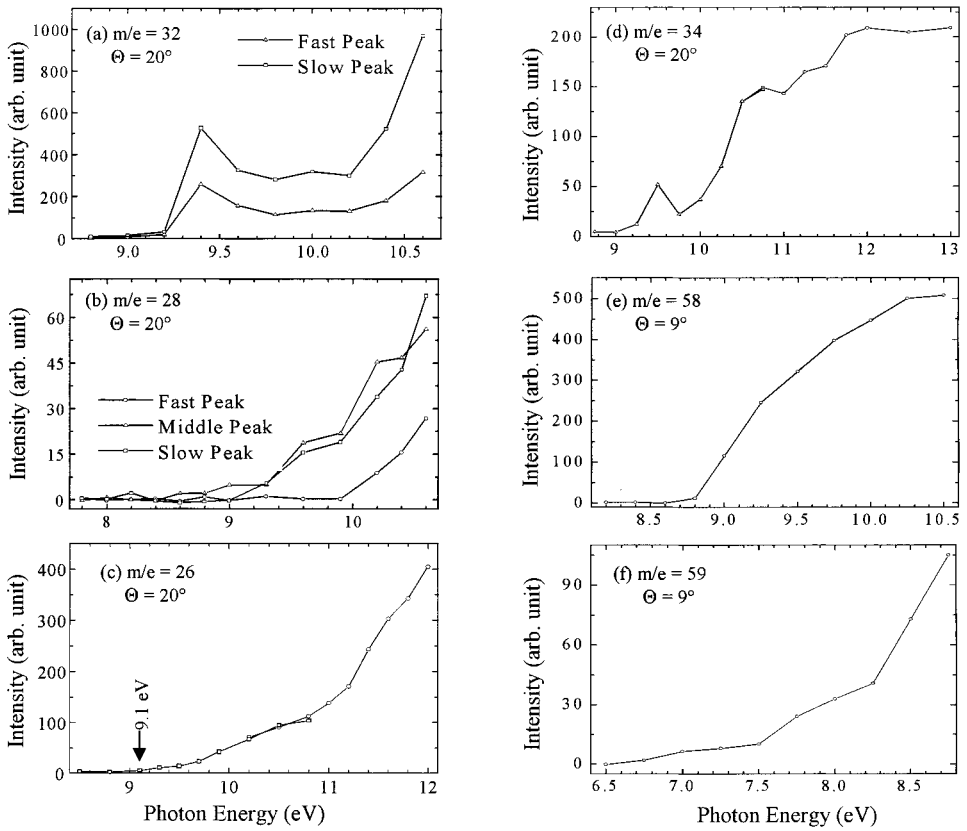

Figure 14. Photoionization efficiency (PIE) spectra of mass 32 (a), 28 (b), 26 (c), 34 (d), 58 (e), and 59 (f) with the indicated scattering angles.

of formation for the triplet ethylene ($^3B_{1u}$) to be 70 ± 3 kcal/mol, using the maximum translational energy, the available energy, and the known heats of formation for *c*-C_2H_4S (22.4 kcal/mol)[1] and S(^{3}P) (66.2 kcal/mol).[6] The difference of the heats of formation between the ground state and the triplet excited state is 58 ± 3 kcal/mol, since the heat of formation of C_2H_4 (^1A_g) is 12.54 kcal/mol.[6] This is the first direct experimental derivation of the heat of formation for the triplet state of ethylene. Our experimental result is little different from the theoretical predictions: the ground state of ethylene is more stable than the triplet state by 46,[54] and 64 kcal/mol[7] at their potential energy minima located at twisting angles of 0° (^1A_g), and of 90° ($^3B_{1u}$). Electron energy loss spectroscopy and theoretical calculation revealed that the $1^1A_g \rightarrow 1^3B_{1u}$ vertical transition energy occurred at 97 kcal/mol[23] and 106 kcal/mol,[7] respectively.

Theoretical calculations of ethylene predicted the equilibrium distance (R_{cc}) of the triplet state (1.48 Å) with two perpendicular CH_2 groups and of the ground state (1.321 Å) with planar CH_2 groups.[7] Fowler and co-workers completed a mechanistic study of the electrocyclic ring-opening reaction of *c*-C_2H_4S using ab initio molecular orbital theory with three different basis sets.[27] The average C−C bond length of *c*-C_2H_4S is 1.48 Å based on three different basis sets. This bond length equals to the equilibrium distance (R_{cc}) at the triplet state of ethylene. The torsion motion could be dominant in a dissociation process, and change of the C−C bond length is minor.

We have discussed three C_2H_4 + S channels now. The following channel is also spin-allowed, and energetically accessible via photodissociation at 193 nm:

$$c\text{-}C_2H_4S + h\nu_{193\,nm} \rightarrow C_2H_4\,(^1A_g) + S\,(^1S) \qquad \Delta H_{avai} = 28\ \text{kcal/mol}$$

In fact, this channel was not observed at 193 nm photodissociation. The IP of S(^{1}S) is 7.6 eV,[8] but no signal was observed at photoionization energies below 9.2 eV, which is the IP of S(^{1}D). This observation is supported by measurements of the PIE spectra, shown in Figure 14a. Two sharp onsets, corresponding to the IPs of S(^{3}P) and S(^{1}D), were observed clearly in Figure 14a. Figure 14b shows the PIE curve of mass 28 by integrating different parts. Two onsets were clearly discerned: one is the internally "cold" C_2H_4 with a fast translational velocity and some vibrational excitations. Its onset is shifted from 10.5 to 10.0 eV. Another onset at 9.0 eV is due to the internally "hot" C_2H_4.

4.2. The HS + C_2H_3 Channel. The translational energy distribution for SH + C_2H_3 derived from our PTS study is similar to a previous report,[1] although the bimodal distribution is more clearly observed in the TOF spectra of mass 33. Furthermore, this bimodality is repeated in the TOF spectra of momentum-matched fragment (*m*/*e* = 27). The first electronically excited state (A $^2\Sigma^+$) of HS is 88 kcal/mol above the ground state, which rules out the formation of HS (A $^2\Sigma^+$) and C_2H_3 ($\tilde{X}\ ^2A'$),[60] since the excitation energy is fixed at 148 kcal/mol. On the other hand the channel producing the first electronically excited state of C_2H_3 in combination with ground state HS is energetically accessible via photodissociation at 193.3 nm:

$$c\text{-}C_2H_4S + h\nu_{193\,nm} \rightarrow C_2H_3(\tilde{A}\ ^2A'') + HS(X\ ^2\Pi) \qquad \Delta H_{avai} = 20\ \text{kcal/mol} \quad \text{(II)}$$

The first excited state of C_2H_3 is 46.0 kcal/mol above the ground

(60) Schnieder, L.; Meier, W.; Welge, K. H.; Ashfold, M. N. R.; Western, C. M. *J. Chem. Phys.* **1990**, *92*, 7027.

state.[61] However, the maximum translational energy for this channel was measured to be 43 kcal/mol. Hence, the 193 nm photodissociation of *c*-C_2H_4S is unlikely to form the excited state of the vinyl radical.

The difference between the two peaks in Figure 3d is about 1014 cm^{-1}. This bimodality may be a result of a vibrational progression of HS or C_2H_3. A series of vibrational peaks of HS were clearly observed in the VUV photodissociation studies of H_2S by several groups.[62−66] The measured SH vibrational frequency is more than 2600 cm^{-1}, and the spin−orbit splitting in the ground state of SH ($^2\Pi_i$) is about ∼377 cm^{-1}.[62,67] Hence the bimodal nature is unlikely to represent vibrational or spin−orbit states of HS. The vinyl radical is one of photoproducts from VUV photodissociation studies of vinyl chloride and ethylene.[59,68] However, TOF spectra of mass 27 did not show any vibrational structure in previous PTS studies.[1] A theoretical calculation predicted three vibrational frequencies of the ground-state vinyl radical at 735, 1062, and 1252 cm^{-1}.[69] So the observed bimodality could be the excitation of the ν_2 vibrational mode or mixed vibrations of vinyl radical.

The HS + C_2H_3 channel likely proceeds on the ground electronic state following intersystem crossing. The energy profile of this channel is shown in Figure 12c. *c*-C_2H_4S first undergoes ring-opening reaction via **TSc**, then it undergoes hydrogen transfer and intersystem crossing to form the final products C_2H_3 ($^2A'$) + HS via **TSd**. The G3 barrier and heat of reaction are 84.4 and 82.6 kcal/mol, respectively, again in good agreement with the estimated experimental barrier (86 ± 1.5 kcal/mol) and heat of reaction (82 ± 1 kcal/mol).

4.3. The H_2S + C_2H_2 channel. A channel producing H_2S with C_2H_2 was observed in this study. The obvious question here is whether the $m/e = 26$ product is HCCH, acetylene, or H_2CC:, vinylidene. The fact that little of the available energy appears in translation for this process, and that the maximum observed translational energy is consistent with exclusive formation of vinylidene, might lead one to make this assignment for the H_2CC: product. The ab initio calculations, however, shed valuable insight into this process. On the basis of G3 calculations, the energy profile of this channel is shown in Figure 12d: *c*-C_2H_4S undergoes hydrogen transfer to form acetylene, first with hydrogen migration via **TSc**, then with a second H migration via **TSe,** clearly a 1,2-H elimination process. No analogous direct pathway involving 1,1-H elimination was found. The question then becomes why so little of the energy of the barrier **TSe** appears in product translation. The answer to this may be found in the fact that the C_2H_2 in this structure bears little resemblance to the acetylene equilibrium structure, and the energy of this highly strained species is not likely to be available to translation as the system relaxes in the exit channel. The result is a translational energy distribution that misleadingly suggests a 1,1-H elimination process, but in fact represents 1,2-H elimination resulting in a strongly bent C_2H_2 product formed at very similar energies to H_2CC:. PIE spectra of mass 26 and 34 were measured and are shown in Figure 14c, d. Both onsets are red-shifted, which means both fragments carrying a lot of internal energy.

4.4. The H atom Elimination Channel. The H atom elimination channel was observed by measuring TOF spectra of $m/e = 59$. Here, tunable synchrotron radiation was used to ionize the fragment with a MgF_2 window. Felder and co-workers measured this channel by recording TOF spectra of the H atom using electron impact ionization. The translational energy distribution derived from our measurement is more direct, since only the process of interest contributes to the observed distribution. The heat of formation of the C_2H_3S radical is derived to be 70 ± 2 kcal/mol from the $E_{max-tran}$ observation, in good agreement with the G3 heats of formation of 72.1 and 69.9 kcal/mol at 0 and 298 K, respectively.

We have calculated the **TS** and the corresponding activation energy for this channel on the ground state. The calculated activation energy for **TS** is 106.1 kcal/mol; however, the experimental value is derived to be roughly 128 kcal/mol from $P(E_T)$ of Figure 3f. This radical has enough internal energy to undergo secondary dissociation. In fact, a strong signal of mass 58 was observed; its TOF spectrum is shown in Figure 8b. A translational energy distribution (Figure 8c) was used to fit the data with a peak at about 4 kcal/mol. Furthermore, PIE spectra of C_2H_2S and C_2H_3S were measured and are shown in Figure 14e, f, respectively. The onset of C_2H_2S is very similar to one found in our previous study.[50] The ionization potential of C_2H_3S is estimated to be about 7.0 eV. If considering the secondary dissociation of C_2H_3S, the $P(E_T)$ in Figure 8c indicates an exit barrier of approximate 3.8 kcal/mol. The reaction barrier was derived to be roughly 106.8 kcal/mol from the heats of formation of C_2H_4S (22.4 kcal/mol), C_2H_3S (72.1 kcal/mol), H (52.1 kcal/mol) and the exit barrier of secondary dissociation. It is also in good agreement with the theoretical predication.

Another possible process to form C_2H_2S is the H_2 elimination channel. The available energy for this process (*c*-$C_2H_4S + h\nu_{193\ nm} \rightarrow C_2H_2S + H_2$) is 122 kcal/mol. We would expect to detect very fast signal of $m/e = 58$ if this process were to happen. But the TOF spectra in Figure 8b do not show any distinct signal at the fast part. Hence, we exclude H_2 elimination as a major channel from 193 nm photodissociation of ethylene sulfide.

5. Conclusions

This study on Endstation 1 at the Chemical Dynamics Beamline of the ALS exploits the tunable vacuum ultraviolet undulator radiation as a *universal* but *selective* probe of the reaction to reveal new aspects of the photodissociation dynamics of ethylene sulfide. This study has shown some important new results, in addition to the established products (process **I′**, **II**, and **IV**). Selective probing allows discrimination of the singlet and triplet components of these distributions. The main conclusions are summarized as the following:

(1) Branchings between the channels, S(^{1}D) + C_2H_4(^1A_g), and S(^{3}P) + C_2H_4(^1A_g), were found to be nearly equal, with the bulk of the ground-state S atom product resulting from a spin-forbidden process.

(2) The second peak around ∼52 μs of the ground-state sulfur atoms is tentatively assigned to the coproduction of the excited *triplet* state $^3B_{1u}$ of ethylene (process **I″**). Furthermore, an upper limit to its heat of formation was derived to be 70 ± 3 kcal/mol. The energetics for process **I″** can be used to provide the first experimental insight into the properties of *triplet* ethylene near its equilibrium geometry.

(61) Wodtke, A. M.; Hintsa, E. J.; Somorjai, J.; Lee, Y. T. *Isr. J. Chem.* **1989**, *29*, 383.
(62) Xie, X.; Schnieder, L.; Wallmeier, H.; Boettner, R.; Welge, K. H. *J. Chem. Phys.* **1990**, *92*, 1608.
(63) Continetti, R. E.; Balko, B. A.; Lee, Y. T. *Chem. Phys. Lett.* **1991**, *182*, 400.
(64) Veen, G. N. A. V.; Mohamed, K. A.; Baller, T.; Vries, A. E. D. *Chem. Phys.* **1983**, *74*, 261.
(65) Weiner, B. R.; Levene, H. B.; Valentini, J. J.; Baronavski, A. P. *J. Chem. Phys.* **1989**, *90*, 1403.
(66) Xu, Z.; Koplitz, B.; Wittig, C. *J. Chem. Phys.* **1987**, *87*, 1062.
(67) Krautwald, H. J.; Schnieder, L.; Welge, K. H.; Ashfold, M. N. R. *Faraday Discuss. Chem. Soc.* **1986**, *82*, 99.
(68) Blank, D. A.; Sun, W. Z.; Suits, A. G.; Lee, Y. T.; North, S. W.; Hall, G. E. *J. Chem. Phys.* **1998**, *108*, 5414.
(69) Paddon-Row: M. N.; Pople, J. A. *J. Phys. Chem.* **1985**, *89*, 2768.

(3) A bimodal distribution was found for the channel of C_2H_3 + HS. This bimodal nature is assigned to different vibrational states of the C_2H_3 radical.

(4) A channel representing the production of H_2S with C_2H_2, was observed, and assigned, on the basis of ab initio calculations, to a 1,2-H elimination process.

G3 calculations and the time-dependent (TD)DFT method were used to elaborate and interpret the dissociation processes of ethylene sulfide at 193 nm excitation. Experimental results are in very good agreement with the theoretical calculations.

Acknowledgment. The authors would like to thank Professor L. J. Butler, Professor D. M. Neumark and Professor T. Baer for helpful discussions. This work was supported by the Director, Office of Science, Office of Basic Energy Sciences, Chemical Sciences Division of the U.S. Department of Energy under Contract No. DE-AC03-76SF00098. The Advanced Light Source is supported by the Director, Office of Science, Office of Basic Energy Sciences, Materials Sciences Division of the U.S. Department of Energy, under the same contract. S.H.C. and W.K.L. are grateful to the Computer Service Center at the Chinese University of Hong Kong for generous allocation of computer time on the SGI Origin 2000 High Performance Server.

JA003314V